Tribol Lett (2014) 54:297–308
DOI 10.1007/s11249-014-0334-z

ORIGINAL PAPER

On the Friction of Carbon Black- and Silica-Reinforced BR and S-SBR Elastomers

Milad Mokhtari · Dirk J. Schipper · Tetyana V. Tolpekina

Received: 24 December 2013 / Accepted: 8 April 2014 / Published online: 23 April 2014

Abstract Friction of carbon black- and silica-reinforced elastomers is studied experimentally and theoretically, using Persson's model. The effect of reinforcement fillers on elasticity was determined by dynamical mechanical analysis. Carbon black-filled samples have a higher Young's modulus than the silica-filled compounds. Silica-filled rubbers have a higher tan (δ) at lower temperatures and a lower loss tangent at higher temperatures, which is a rough indication for higher wet grip and lower rolling resistance, respectively. Friction tests on a ball-on-disk test rig were performed to study the effect of the reinforcement fillers and their amount on the friction between rubber samples (disks) and relatively smooth or rough granite surfaces (balls). The results were discussed and compared with the friction model presented by Persson. It was shown theoretically and experimentally that hysteresis does not play a significant role in the friction of rubber samples in contact with smooth granite and that it plays a minor role in contact with a rough granite sphere. Therefore, the hysteresis contribution of friction can be neglected in the contact of rubbers with just smooth spheres. Moreover, a higher friction coefficient is seen in samples with a higher content of fillers. Silica-filled compounds show a slightly higher coefficient of friction compared with the carbon black-filled compounds. The effect of attached wear debris to the granite surfaces on the friction level has been studied. The results are supported by SEM and confocal microscopic images of the wear debris itself and wear debris attached to the granite spheres, respectively.

Keywords Friction · Elastomer · Hysteresis · Real area of contact · Interfacial layer

M. Mokhtari (✉) · D. J. Schipper
Surface Technology and Tribology, Faculty of Engineering Technology, University of Twente, P.O. Box 217, 7500 AE Enschede, The Netherlands
e-mail: m.mokhtari@utwente.nl; mokhtari.ac@gmail.com

T. V. Tolpekina
Apollo Tyres Global R&D B.V., Colosseum 2, 7521 PT Enschede, The Netherlands

List of symbols

F_f	Total friction force (N)
F_{vis}	Hysteresis contribution of friction force induced by viscoelastic losses (N)
$\tau_f(v)$	Frictional shear stress as a function of velocity (Pa)
$A(v)$	Real area of contact as a function of velocity (m^2)
μ_f	Total coefficient of friction
F_N	Nominal normal load (N)
σ_0	Nominal contact pressure (Pa)
A_0	Nominal area of contact (m^2)
μ_{vis}	Viscoelastic or hysteresis coefficient of friction
$P(q)$	Real to the nominal area of contact ratio as a function of wave vector
ω	Frequency of the applied load to the rubber (rad/s)
λ	Length scale of the roughness under study (m)
$\vec{q}$	Roughness wave vector (1/m)
q	Amplitude of the roughness wave vector (1/m)
q_0	Lower wave vector cutoff corresponding to the longest wave length of roughness (1/m)
q_1	Higher wave vector cutoff corresponding to the shortest wave length of roughness (1/m)
$C(q)$	Power spectral density of the roughness (m^4)
$A(q)$	Apparent contact area when the surface is smooth on all wave vectors $>q$ (m^2)
ϕ	Angle between the velocity vector and the wave vector $\vec{q}$ (rad)
E	Modulus of elasticity (Pa)
$G(\omega)$	The shear modulus (Pa)

v	Poisson's ratio
τ_c	Effective frictional stresses with regard to energy dissipation at a crack opening (Pa)
τ_s	Effective frictional stresses with regard to shearing a thin confined film (Pa)
$G(v)$	Energy/area to break the interfacial rubber–substrate bond as a function of velocity (w/m^2)
a	Crack-tip radius (m)
a_T	The temperature–frequency viscoelastic horizontal shift factor
T_g	Glass transition temperature (°C)
ξ	Magnification factor

1 Introduction

The interaction between tire and road determines whether sufficient traction is present under wet and dry conditions [1–3] as well as the amount of noise radiation [4], energy losses [5], vibration [6] and rubber particles production [7]. Providing adequate grip between tire and road while simultaneously minimizing the undesirable effects of the tire–road interaction has been the subject of several researches in the past decades [8–10]. Solving the aforementioned problem seems impossible unless the main mechanisms responsible for the tire–road interaction are well understood. Friction of polymers against solid surfaces is one of the most important mechanisms engaged in the tire–road interaction. Rubber seals, wiper blades, conveyor belts and syringes are some practical applications that require sufficient knowledge on rubber friction. Although great interest has been kindled by studying the tribological behavior of rubber sliding contacts in the past 50 years [11–13], the friction problem is not yet fully understood.

Several parameters such as contact pressure, (sliding) velocity, temperature and surface roughness, as well as morphology of the rubber compounds, play a role in the friction of polymers in contact with solid surfaces and, as a consequence, modeling rubber friction is not a simple task. The friction of polymers in contact with a solid surface differs from friction of other solids and simple friction models, such as the Coulomb's friction law, are not adequate to describe friction under different conditions. Historically, the friction force between rubber and a rough surface was considered as a summing up of two main contributions, commonly described as the adhesion and hysteresis components [14]. The intermolecular attractive forces between the contacting bodies are considered as the mechanism responsible for the adhesion [15]. On the other hand, cyclic deformation of the rubber, caused by exerted oscillating forces of asperities of a rough surface, dissipates energy and generates the hysteresis component of friction [16]. There has been an ongoing debate among researchers on the question of which component plays the major role in the overall friction. In the early works of Persson [17], the hysteresis was assumed to be the main contributor of rubber friction, while Le Gal and others [1] found that adhesion plays a dominant role. In a recent paper of Lorenz et al. [18], some other contributors to rubber friction are considered: energy dissipation due to crack opening and energy dissipation in shearing a thin viscous film [3]. Pan emphasizes the significance of interfacial interactions in determining the wet sliding friction of elastomer compounds in his research [19]. Moreover, a contribution to rubber friction as a result of wear processes is also mentioned and not well studied yet [3, 18].

The problem gets even more complicated by adding different fillers to the rubber compound. The effect of different fillers in rubber friction is of interest from a scientific point of view as well as for industrial applications, especially the tire industry. Silica and carbon black have been used as the main reinforcing agents in rubber compounds. It has been reported that substitution and/or addition of silica to carbon black-filled rubbers may modify the wet grip behavior as well as the rolling resistance of tires [19, 20]; however, much less is known about the mechanism responsible for this.

This paper studies the effect on friction of carbon black and silica, as reinforcement fillers, using a mixture of butadiene rubber (BR) and solution styrene-butadiene rubber (S-SBR) against rock (granite) based on a combined experimental–theoretical approach and tries to find the main contributor in friction.

The outline of this paper is as follows: In Sect. 2, the basic equations developed by Persson are presented, which are used to calculate the friction of rubber in contact with a solid rough surface. Section 3 starts with the materials used in the experiments and discusses DMA measurements performed to determine the mechanical characteristics of the rubber samples. Then, the results of the friction tests are discussed. Section 4 contains the numerical results based on the equations presented in Sect. 2. In Sect. 5, the results of Sect. 4 are used to explain the results of Sect. 3 and different aspects of the results are discussed. Finally, in Sect. 6, the main conclusions are given.

2 Rubber Friction

The model developed by Persson is used to calculate the friction. Friction is modeled by incorporating the contributions of the roughness-induced viscoelastic deformation

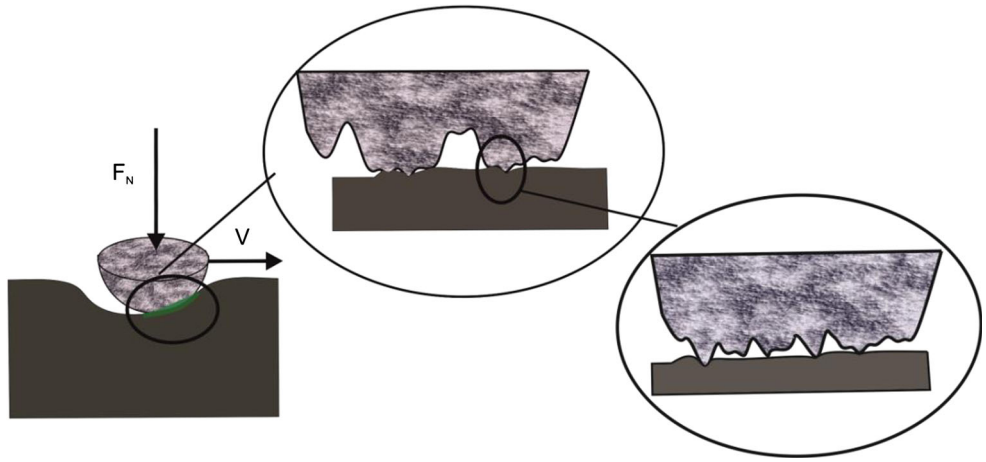

Fig. 1 Sphere in sliding contact with rubber is shown schematically. All the surfaces are rough and many length scales are involved in the roughness and consequently, the friction [16]. The contribution from the area of contact in total friction is shown by the *green color* in nominal contact area, while the real area of contact is a function of magnification. The real area of contact decreases with an increase in magnification. Two magnifications are shown in the figure. Evidently, the contribution from the area of contact is just applied to the real area of contact and not to noncontact areas (Color figure online)

of the rubber as well as the contribution from the area of contact [3, 18]:

$$F_{\mathrm{f}} = F_{\mathrm{visc}} + \tau_{\mathrm{f}}(v)A(v) \quad \text{or}$$
$$\mu_{\mathrm{f}} = \frac{F_{\mathrm{f}}}{F_{\mathrm{N}}} = \frac{F_{\mathrm{visc}}}{\sigma_0 A(0)} + \frac{\tau_{\mathrm{f}}(v)A(v)}{\sigma_0 A(0)} \tag{1}$$

where σ_0 and A_0 are the nominal contact pressure and contact area, respectively. F_{visc} is the friction force related to the hysteresis losses in the bulk of the material that originates from the viscoelastic nature of the rubbers, $A(v)$ is the real area of contact as a function of velocity, $\tau_f(v)$ is the frictional stress due to the contribution from the area of contact and F_f is the total friction force in contact between the rubber and a rigid surface. Rubber friction contributors are shown schematically in Fig. 1.

2.1 Hysteresis Component of Friction

The hysteresis component of the friction is originated from the oscillating forces that the surface asperities exert onto the rubber surface. These forces lead to cyclic deformations and energy dissipation due to internal frictional damping. The asperities of a rigid solid, with a sinusoidal rough surface with period l, exert a fluctuating force with a characteristic frequency $\omega = v/l$ to a rubber solid if the relative velocity between the rubber block and the rigid surface is equal to v. Surfaces are rough with roughness on many different length scales λ [21]; therefore, the contribution to rubber friction from the viscoelastic deformation (and consequently hysteresis losses) of the rubber surface exerted by the substrate asperities depends on the frequency-dependent viscoelastic modulus $E(\omega)$ (see Sect. 3.2, which deals with characterizing and determining the elasticity modulus over a range of frequencies). The asperities and the distribution of length scales λ in the roughness of the counter surface determine the distribution of frequency components in the Fourier decomposition of the surface stresses acting on the sliding rubber. In the model of Persson, the power spectral density of the roughness, $C(q)$, is considered as a function which contains all the necessary information regarding oscillating exerted forces from asperities. The definition and calculation method of the power spectral density of a rough surface can be found in [21] where q is the amplitude of the wave vector related to the wavelength λ by $q = 2\pi/\lambda$. Friction is also a function of (flash) temperature as a consequence of heat generated as a result of loss of energy in the contact. In this research, low velocity in the contact of rubber with the rigid surface is considered, so the influence of flash temperature on friction is neglected.

The real area of contact is much smaller than the apparent area of contact A_0. As an example, the real area of contact between the tire and the road is typically only ~ 1 % of the nominal footprint contact area [16]. The real area of contact is important because it plays a role in determining the friction. Persson defines the real area of contact as a function of length scale λ, where the surface would be smooth on all length scales shorter than λ. The basic equations of the hysteresis coefficient of friction as well as the real area of contact are summarized below [16, 18]:

$$\mu_{\mathrm{vis}} \approx \frac{1}{2}\int_{q_0}^{q_1} \mathrm{d}q\, q^3 C(q) P(q) \int_0^{2\Pi} \mathrm{d}\phi \cos\phi\, \mathrm{Im}\left[\frac{E(qv\cos\phi)}{(1-\nu^2)\sigma_0}\right], \tag{2}$$

where the function $P(q) = {}^{A(q)}/_{A_0}$ is given by

$$P(q) = \frac{2}{\Pi}\int_0^{\infty} \mathrm{d}x \frac{\sin x}{x}\exp\left[-x^2 G(q)\right], \tag{3}$$

where

$$G(q) = \frac{1}{8}\int_{q_0}^{q} \mathrm{d}q\, q^3 C(q) \int_0^{2\Pi} \mathrm{d}\phi \left|\frac{E(qv\cos\phi)}{(1-v^2)\sigma_0}\right|^2. \tag{4}$$

$A(q)$ is the apparent area of contact if the surface were smooth for all wave vectors larger than q, A_0 is the nominal contact area at the shortest wave vector q_0 and x is an integration variable. It should be noted that it is assumed that rough surfaces are isotropic, so just the amplitude of the wave vector $|\vec{q}| = q = 2\pi/\lambda$ is important and not its direction where λ is the considered wavelength of the roughness. The theory is presented in the general form and is valid for all surfaces; however, the formulations can become simpler if the surface is self-fractal for $q_0 < q < q_1$ where the limitations are defined by the shortest and longest wavelengths of the roughness studied. ϕ is the angle between the velocity vector and the wave vector $\vec{q}$, σ_0 the nominal contact pressure and v the Poisson's ratio. For an extended definition of the parameters, see [16, 17].

2.2 Real Area of Contact Contribution

Two different physical phenomena are responsible for the contribution of the real area of contact to the overall friction, $\tau_f(v) = \tau_c(v) + \tau_s(v)$ where τ_c and τ_s are the effective frictional stresses with regard to energy dissipation at a crack opening and shearing a thin confined film, respectively.

Dissipation of energy at the crack openings results in the effective frictional stress τ_c acting at the real area of contact. The energy per unit area required to break the interfacial rubber–substrate bonds is called $G(v,T) = G_0[1 + f(v,T)]$ which is a function of crack-tip velocity v and the temperature T. G_0 is the energy to break the interfacial rubber–substrate bonds at extremely low crack velocities. If one assumes that the contact area consists of N regions of average size l (i.e., $A = Nl^2$), then the following balance of energy is satisfied during a sliding distance of dx:

$$\tau_c A\mathrm{d}x = G(v)Nl\,\mathrm{d}x \quad \text{or} \quad \tau_c = \frac{G(v)}{l} = \frac{G(v)}{G_0}\frac{G_0}{l}. \tag{5}$$

The dissipated energy as a result of crack propagation in high velocities for a viscoelastic solid is caused by hysteresis losses. The perturbing frequency is related to the distance r from the crack tip. The crack-tip radius a is recognized as the smallest possible r. Hence, the highest possible frequency will be ${}^{v}/_{a}$ (see [22] for more details). It is shown in [22] that,

$$G(v)/G_0 = \left[1 - {}^{2}/_{\pi}E_0 \int_0^{2\Pi v/a} \mathrm{d}\omega \frac{F(\omega)}{\omega}\mathrm{Im}\left[\frac{1}{E(\omega)}\right]\right]^{-1}, \tag{6}$$

where $E_0 = E(\omega = 0)$, a is the crack-tip radius and $F(\omega) = \left[1 - \left(\frac{\omega a}{2\pi v}\right)^2\right]^{1/2}$. The crack-tip radius cannot be smaller than an atomic diameter; therefore, in references [18, 22], $a_0 = 1$ nm is proposed and used. Because of difficulties in calculating the integral in Eq. 6 (originated from broad frequency range that extends over many decades), a simpler method is proposed [18, 22].

The second physical phenomenon dealing with the real area of contact contribution in the overall friction is due to the force of shearing a thin fluid-like film formed by segments of rubber molecules [3, 18]. Persson has suggested using,

$$\tau_s = \tau_0(a_T v)^{\alpha}, \tag{7}$$

where a_T is the temperature–frequency viscoelastic shift factors and τ_0 is basically a fitting parameter. One can find more about the origin of the formulas in [18].

It is mentioned in [3, 18] that wear can also play a role in the friction of rubbers against solid surfaces; however, it was not further developed. Some simple models do exist that have considered the contribution and the effect of wear in the total friction [23] and, specifically, the friction of polymers [24]. In this research, in Sect. 5, the role of wear on the total friction is studied based on an experimental approach.

3 Experimental

3.1 Materials

The rubber samples employed in this study include 30 parts per hundred rubber (phr) butadiene rubber (BR) and 70 phr solution styrene-butadiene rubber (S-SBR). The samples are mixed with two different filler systems, carbon black (N375) and silica. The compounds are prepared by varying the amount of fillers, namely 100, 85 and 70 phr of carbon black or silica. For silica-filled compounds, depending on the amount of silica, the amount of processing oil needed to functionalize and disperse the silica particles was varied. Bifunctional organosilanes, such as bis(triethoxysilylpropyl)-tetrasulphide (TESPT), are used (depending on the silica content) to chemically modify the silica surfaces to enhance the compatibility of hydrocarbon rubbers and

Table 1 Different rubber compounds prepared with the amounts of components indicated in phr where HC: high carbon black content, MC: medium carbon black content, LC: low carbon black content, HS: high silica content, MS: medium silica content and LS: low silica content

Compound	HC	MC	LC	HS	MS	LS
Description	phr	phr	phr	phr	phr	phr
BR, high cis	30	30	30	30	30	30
SSBR	70	70	70	70	70	70
N375	100	85	70	–	–	–
Silica	–	–	–	100	85	70
TESPT	–	–	–	7.8	6.63	5.5
Processing oil	31	17	4	31	21	17
Sulfur	1.3	1.3	1.3	1.3	1.3	1.3
TBBS	1.3	1.3	1.3	1.3	1.3	1.3
DPG	2	2	2	2	2	2
ZnO	3	3	3	3	3	3
Stearic acid	2	2	2	2	2	2
PVI	0.2	0.2	0.2	–	–	–
Anti-aging chemicals	6	6	6	6	6	6
Zinc salt of fatty acids	3	3	3	3	3	3

precipitated silica by modifying the surface of the silica. An overview of the different rubber compounds prepared with the corresponding amounts (phr) of the components is given in Table 1.

In this paper, we refer to the samples as HC, MC, LC, HS, MS, LS which correspond to high, medium and low contents of carbon black (C) and silica (S), respectively.

3.2 Viscoelasticity of Compounds

The glass transition temperature of the samples is determined using dynamical mechanical analysis (DMA) in temperature sweep mode at a fixed frequency of 10 Hz under dynamic and static strains of 0.1 and 1 %, respectively. Then, the shear modulus $G(\omega)$ is measured in oscillatory shear mode at a constant strain amplitude of 0.1 % where the sample is fixed at both interfaces and sheared at different frequencies between 1 and 200 Hz. The whole procedure is repeated then for different temperatures (the temperature is varied between −20 and 85 °C). The measured glass transition temperature and the selected reference temperature $T_{\text{ref}} = 27$ °C are used to shift the measured shear modulus $G(\omega)$ against frequency ω both horizontally and vertically; Based on the time–temperature superposition principle, the effect of changing the temperature and applying a multiplication factor a_T to the time scale is similar; therefore, the measured shear modulus in a limited frequency range ($1 < f < 200$ Hz) can be used to

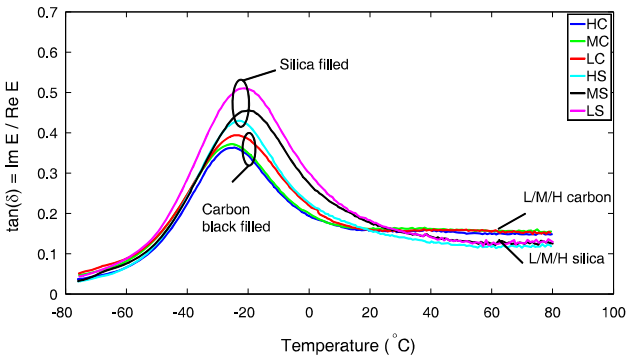

Fig. 2 Loss tangent as a function of temperature for six different filled compounds

estimate the modulus at high frequencies [25]. Williams–Landel–Ferry (WLF) equation presented below is applied for the horizontal shifting: $\log f_h = \frac{-C_1(T-T_{\text{ref}})}{C_2+T-T_{\text{ref}}}$, where C_1 and C_2 are two constants that depend on the elastomer as well as the selected reference temperature. Construction of broad frequency scale master curves from the limited measured modulus is only feasible for amorphous, unfilled rubbers [26] where the rubber behaves linearly. A necessary condition for using the shift factors of the unfilled systems for a filled compound is that the filler does not influence the location of the glass transition [27, 28]. This is the case for all six studied samples (see Figs. 2, 3). Considering the fact that all the samples are filled with different fillers and filled rubbers show nonlinear viscoelastic behavior, only horizontal shifting cannot provide a continuous broad master curve; therefore, a vertical shifting should be also employed to shift the measured data along the vertical axis. The reasons of failure of the WLF equation for filled samples are mentioned in Ref. [27]. Vertical shifting is performed in some other researches [1, 28].

In tire application, deformations can be of the order of 100 %; therefore, the measurements should be performed at high strains; however, the rubber has a nonlinear behavior at high strains where the WLF relation is not valid; therefore, our measurements were performed at lower strains. The authors are aware of the effect of the strain softening in rubbers where the elasticity modulus might decrease at higher strains. A new procedure for shifting is proposed by Lorenz et al. [29]. However, it is not possible at this moment to conduct direct measurements for high strains that correspond to the tire application and high frequencies at the same time. Therefore, there is no direct validation which method is the best for making master curves.

The measured loss tangent, which is the ratio between the loss and storage modulus of the samples as a function

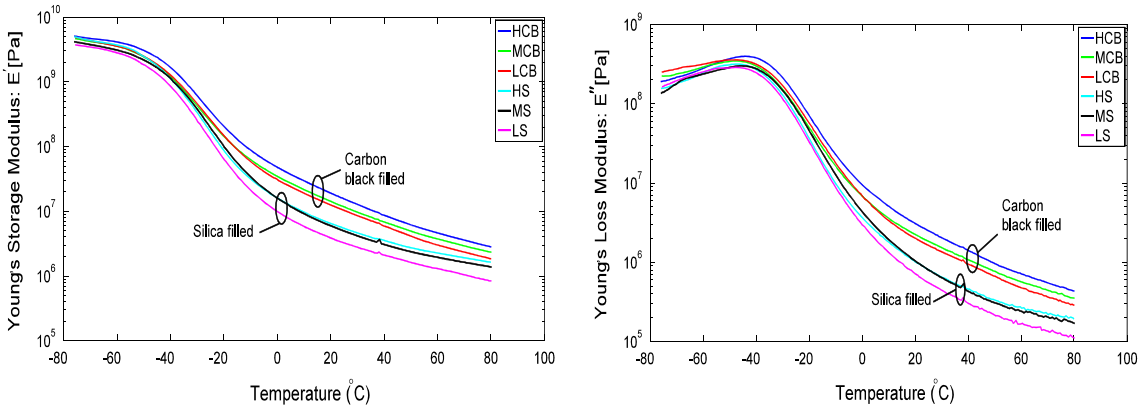

Fig. 3 Young's storage (*left*) and loss (*right*) modulus of elasticity as a function of temperature for different samples

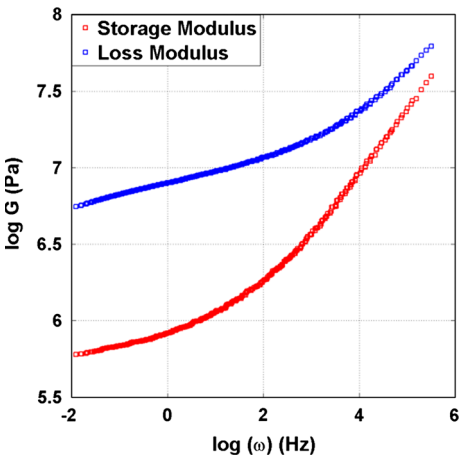

Fig. 4 Shifted loss and storage shear modulus of elasticity as a function of frequency for 85 phr silica-filled rubber

of temperature, is plotted in Fig. 2 as shown; the peak of loss tangent is higher for silica-filled compounds compared with the carbon black-filled samples. The phase angle is inversely dependent on the filler content. This trend is discussed in [22].

Moreover, the peak occurs at slightly higher temperatures for silica-filled compounds. Also, the temperature at which the peak value of the tan (δ) occurs decreases with increasing filler content. On the other hand, at higher temperatures ($T > 30$ °C), silica-filled compounds show lower tan (δ).

This result is consistent with the results of other researchers where it has been generally accepted that replacement of carbon black by silica results in a decline of the rolling resistance due to a decrease of tan δ at higher temperatures, while it simultaneously leads to a comparable tan δ at lower temperatures, providing a comparable wet grip [30].

The effect of the filler and its content on the Young's modulus of elasticity is shown in Fig. 3. It can be concluded that the carbon black-filled samples generally possess a higher elasticity than the silica-filled compounds. In addition, the modulus of elasticity is dependent on the filler content.

The calculated master curve for the modulus of elasticity as a function of frequency is shown in Fig. 4 (just for one sample) for the MS rubber.

3.3 Friction Tests

The friction tests are performed by a ball-on-disk setup schematically shown in Fig. 5 and under controlled environmental conditions. The temperature was kept constant at 27 °C and the relative humidity at 50 %. The counter surfaces against the rubber samples are granite balls with a diameter of 30 mm. The sliding velocity was kept constant at 5 mm/s as well as the contact pressure, i.e., 0.4 MPa. A sample of the measured signal is shown in Fig. 5. The coefficient of friction is considered as the mean value when the signal is stabilized; in other words, the running-in friction is neglected.

The granite spheres are prepared with two different roughnesses, namely smooth and rough, i.e., with arithmetic average roughness of 0.52 and 2.28 μm, respectively. The power spectral densities of the spheres are shown in Fig. 6. As is shown in the figure, the granite surfaces are self-fractal and the polished surface is much smoother than the rough one. The granite surfaces used in the present study are smoother than the road roughness but they are comparable with the stones present in the asphalt (that are even polished after some time of usage). Therefore, this study can provide information about the contribution of hysteresis and area of real contact on that roughness level.

The friction measurement results are shown in Fig. 7. In the figure, the average and the standard deviation of the

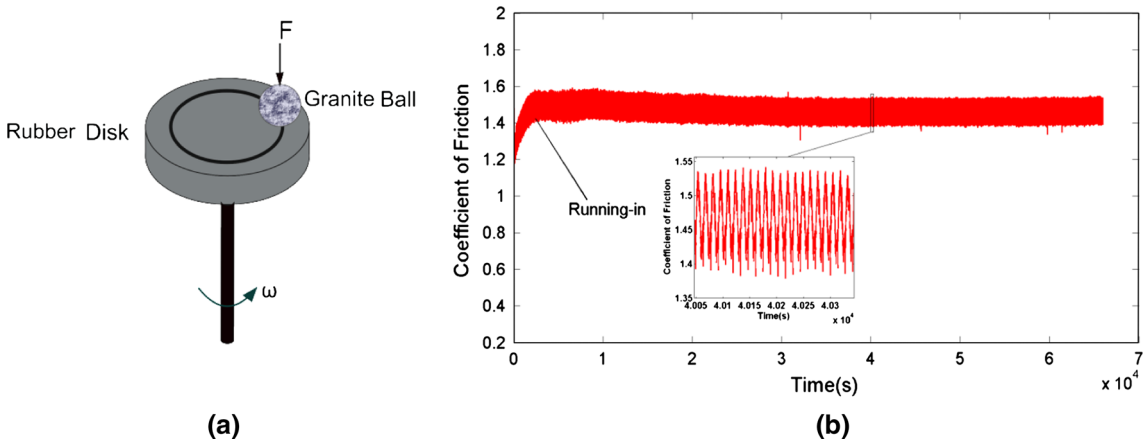

Fig. 5 **a** Ball-on-disk setup used for friction measurements. **b** A sample of measured coefficient of friction versus time. The running-in phase is neglected and the stabilized part is used in determining the friction coefficient. The friction signal repeats itself

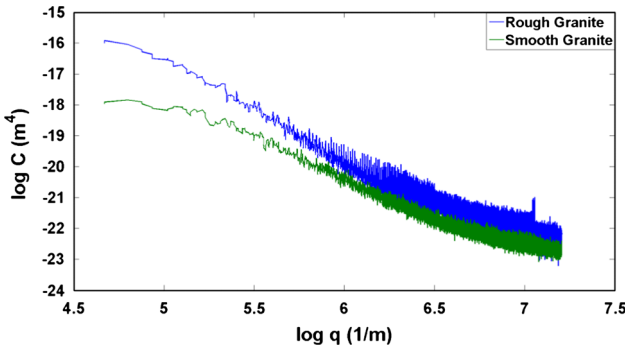

Fig. 6 Power spectral density of roughness for relatively smooth and rough granite spheres

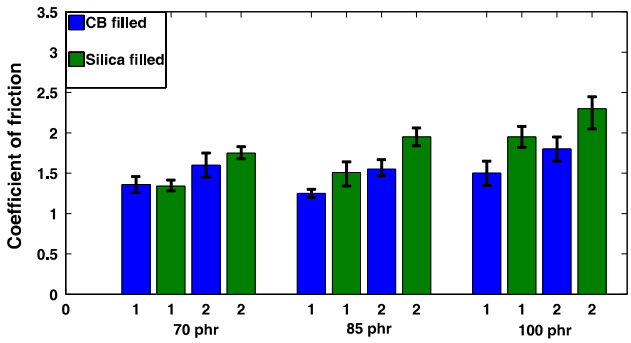

Fig. 7 Coefficient of friction for carbon black- and silica-filled compounds with different filler contents where *1* and *2* indicate the relative rough and smooth counter surfaces roughness condition, respectively

measured friction coefficient is shown. From these measurements, one can conclude that silica-filled compounds have a higher level of friction (except for low filled samples in contact with rough granite where the difference is not sensible) and also, an increase in filler content (for silica-filled rubbers) increases the coefficient of friction as well. Further, smooth surfaces in contact with the rubber samples do produce higher friction forces than rough surfaces. These results are consistent with the numerical calculations of the model results presented below, but to understand the rubber friction in the studied system in more detail, and in order to estimate the contribution of the hysteresis component of the friction in the total friction, a simple measurement was performed. The rubber surface was wetted by a thin layer of oil (Ondina 927 with a dynamic viscosity of 78 m Pa s at 20 °C) such that the lubricated tribosystem remains in the boundary lubrication regime, i.e., no hydrodynamic effects. It was seen that for the smooth ball, the coefficient of friction decreases drastically (as an example, for 85 phr silica-filled rubber from 1.55 to 0.05), showing the limited role of deformation or hysteresis in the overall friction (see Eq. 1). Therefore, the hysteresis component of friction can be neglected when a smooth surface is in contact with rubber. On the other hand, when the relatively rough surface was in contact with the rubbers, although the coefficient of friction dropped to lower values as well (e.g., from 1.3 for low silica-filled compound to 0.5), but because of this value, the effect of hysteresis contribution on friction cannot be neglected. This result is consistent with [3].

4 Numerical Results

Based on Eq. (3) and using the measured roughness, the real area of contact is calculated, for a sliding velocity of $v = 5$ mm/s as a function of the magnification, $\xi = q/q_0$, for the different samples in contact with the relatively smooth and rough spheres. The results are presented in Fig. 8. The shortest wave vector, $q_0 = \frac{2\pi}{L}$, depends on the longest wave length (L) in contact. This can be determined

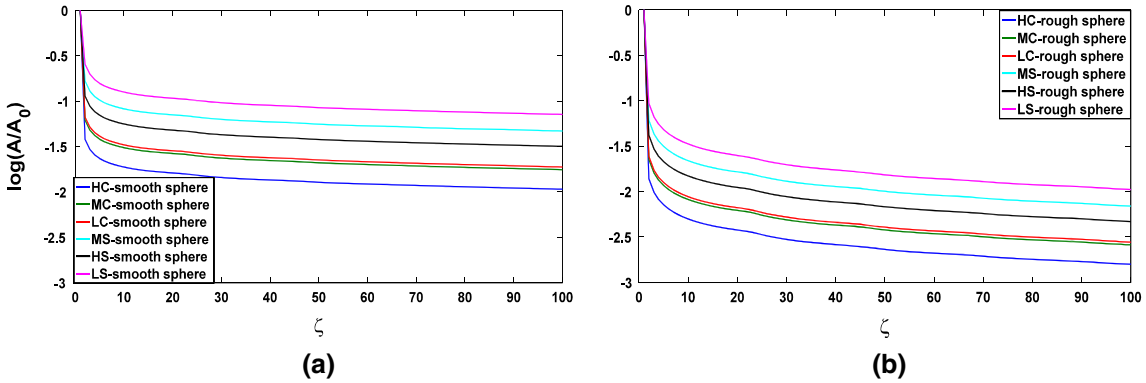

Fig. 8 Variation of real area of contact over nominal contact area as a function of magnification for sliding velocity of $v = 5$ mm/s for rubbers in contact with **a** smooth and **b** rough granite surfaces

by the apparent area of contact. For this purpose, the Hertz contact model is used to calculate the diameter of the contact area for the different samples. The linear size of the contact regions, l, plays a crucial role in calculating the shear stress corresponding to the energy dissipation in crack openings (see Eq. (5)). This value was found to be in relation to the large wave vector cutoff q_1 [18]. As shown in Fig. 8 and Eqs. (2) and (3), the large cutoff wave vector is the determining factor as well in calculating the real area of contact and the hysteresis component of the overall friction. Therefore, the large cutoff wave vector has an effect on the whole analysis. It has been suggested that the size of the road contamination particles (dust or sand particles) could be one of the determining factors in relation to the large cutoff wave vector q_1 [21]. However, for clean surfaces, Persson introduced a yield condition, which is related to an intrinsic property of the rubber, to determine the cutoff wave vector q_1. It is assumed that the local stress and temperature in the asperity contact regions for a length scale $\lambda_1 = \frac{2\pi}{q_1}$ are sufficiently high to break the rubber bonds, so a thin confined layer of rubber with thickness $\approx 1/q_1$ is formed at the rubber surface that is in contact with the counter surface asperities. This process to determine q_1 is closely related to the wear of the rubber samples. However, to determine the optimum cutoff, values of other parameters have to be known in advance, and these values are found in such a way that the numerical results fit properly with the experiments [31]. On the other hand, one can initially fit the experiments with the numerical results to find the optimum value for q_1. The latter procedure is also used to validate Persson's theory [3]. Different values for q_1 are used for different rubber–granite tribosystems to fit with the experiments. The short wavelengths are of the order of $\lambda_1 \approx 0.5$ μm for rough granite spheres in contact with HC sample (λ_1 increases with a decrease in filler content, it is lower for contact of a rough sphere in comparison with contact of a smooth granite sphere with the

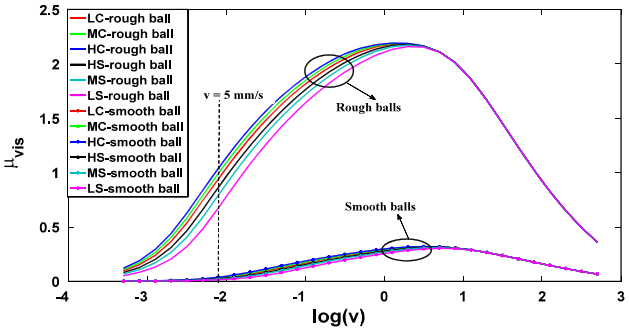

Fig. 9 Hysteresis coefficient of friction as a function of sliding velocity for carbon black- and silica-filled samples in contact with relatively smooth and rough spheres

same rubber and is higher for contact between a silica-filled than carbon black-filled rubber and similar sphere) and of the order of $\lambda_1 \approx 8$ μm for smooth granite spheres in contact with LS rubber (see also Fig. 11 and the difference in the size of the carbon black- and silica-reinforced rubber debris). The short wavelengths selected for all other tribosystems vary between these two values and increases as explained above. These values are of the order of the short wavelengths used or measured in the different rubber systems with rough and smooth surfaces such as concrete, sandpaper or asphalt roads [1, 18, 22, 32].

Figure 8 shows that, as expected, the area of real contact decreases with an increase in the Young's modulus of elasticity (as a result of an increase in the filler content).

Another interesting result illustrated by Fig. 8 is that the real area of contact for all rubber samples increases approximately 3–5 times when a smooth ball is in contact with rubber compared to the rough one.

The calculated viscous coefficient of friction, based on Eq. (2) for both surfaces in contact with the rubber samples, is shown in Fig. 9 as a function of the sliding velocity.

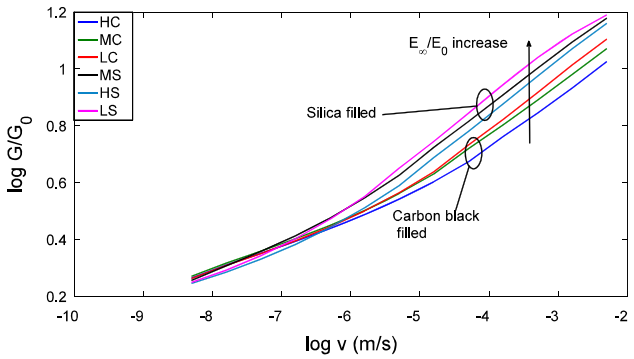

Fig. 10 Crack propagation energy enhancement factor $G(v)/G_0$ as a function of the crack-tip velocity for different samples

The ratio $G(v)/G_0$ (see Eq. 5) is calculated and plotted against velocity v in Fig. 10. In the calculations, the value suggested in [18, 22] for the crack-tip radius for low velocities $a_0 = 1$ nm is used. It has been reported that the measured value for G at extremely low crack velocities is of the order ≈ 0.1 J/m^2 [18]. G_0 values are selected in the same order for the samples used in this research. For "high" crack velocities, $G(v) \approx G_0 \frac{E_\infty}{E_0}$ [1, 22, 33]. The ratio of the dynamic modulus in the glassy state to that in the rubbery state, $\frac{E_\infty}{E_0}$, is higher for silica-filled compounds and is related inversely to the filler content (for both silica and carbon black-filled samples). Figure 10 shows that $G(v)$ increases with an increase in $\frac{E_\infty}{E_0}$. In short, for $v = 5$ mm/s, the carbon black-filled samples show lower energy dissipation (at crack openings) than silica-filled samples and the dissipated energy increases with a decrease in filler content. As a conclusion, the dissipated energy in the crack openings is inversely related to the modulus of elasticity.

The contribution of energy dissipation at crack openings to the overall friction coefficient is $\frac{\tau_c(v)A(v)}{\sigma_0 A(0)}$ (see Eq. 1). The effective frictional stress with regard to energy dissipation at a crack opening, τ_c, is governed by Eq. (5). As it is shown in Fig. 10, $1.1 < \log_{10}\frac{G}{G_0} < 1.2$ (which does not differ severely for different samples), it was mentioned earlier that $0.5 < l < 8$ μm. However, the real area of contact changes drastically for different tribosystems. Substituting the given numbers for each system reveals that dissipation of energy at crack openings for contact of rubbers with rough spheres (and especially carbon black-filled rubbers where $\frac{A(v)}{A(0)}$ is much smaller) is negligible while this phenomenon plays a minor role in total friction for contact of smooth balls with rubbers (especially silica-filled samples which have much higher real contact areas). Moreover, for systems which hysteresis is negligible, dissipation of energy in crack openings plays a minor role in total friction and vice versa. None of these two phenomena can describe the measured friction coefficients. Therefore, shearing of a thin interfacial layer is the main contributor in friction of studied rubber disks and granite balls.

The frictional shear stress τ_0 in Eq. (7) is selected such that the numerical results are in agreement with the measurements. These values are of the order of a few MPa to 22 MPa and with a power $\alpha = 0.05$ in Eq. (7) which are in the range of values found elsewhere [1, 3, 18].

5 Discussion

It is seen that for the samples with a higher modulus of elasticity (higher filler content), the viscous coefficient of friction is just slightly higher. This can be explained by Eq. (2), where the competition between $P(q)$ and the imaginary part of the elastic modulus determines the viscous friction. Although a higher filler content decreases the real area of contact, as is illustrated in Fig. 8, the loss modulus also increases (Fig. 3). It can be observed from Fig. 7 that an increase in the filler content (or modulus of

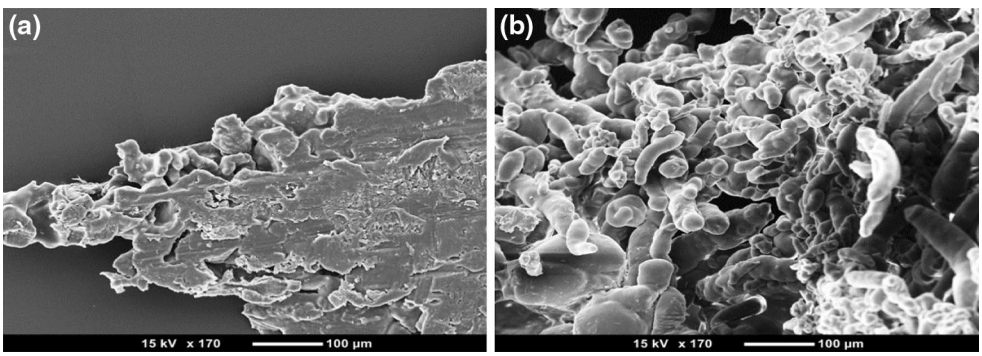

Fig. 11 Scanning electron microscopic pictures of rubber wear particles: **a** wear particle from 85 phr carbon black-filled rubber and **b** wear particle from 85 phr silica-filled rubber

elasticity) results in an increase in the total measured coefficient of friction and stays approximately in the same range for silica and carbon black-filled samples. This increase is the superposition of a slight increase in the viscous coefficient of friction and a decrease in the real area of contact (the contact area decreases 3 to 5 times). This can only be valid if τ_f, presented in Eq. (1), also increases as the filler content increases.

Although dissipation of energy at the crack openings plays a role in the overall friction, it is not the main contributor. When rubbers are in contact with rough surfaces, the real area of contact is much smaller; however, it plays a minor role in contact with smooth counter surfaces.

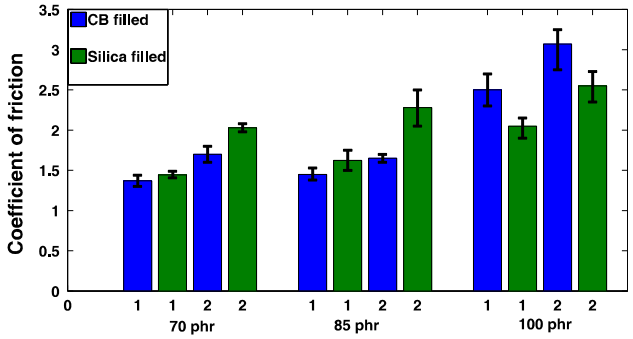

Fig. 12 Coefficient of friction for carbon black- and silica-filled compounds with different filler contents in contact with contaminated granite surfaces where *1* and *2* indicate the relative rough and smooth counter surfaces roughness condition, respectively

Moreover, for smooth surfaces and when no debris is attached to the counter surface, adhesional interaction might also increase the area of real contact contribution. For rough surfaces, the hysteresis component of friction together with friction induced by shearing a thin interfacial layer explains the levels of the measured friction, while for the smooth surfaces, shearing of a thin interfacial layer plays the dominant role and the energy dissipation at crack openings just slightly contributes to the overall friction. The strain softening effect might result in higher areas of real contact which brings about lower values for τ_0 than the calculated shear stresses. This shows the importance of studying the origin of τ_0 and not considering it just as a fitting parameter which has not been performed yet. Therefore, a more detailed theoretical–experimental approach is required to acquire sufficient knowledge on the properties of the interfacial rubber surface layer.

Studying the wear debris of the different rubber samples shows that the wear debris of carbon black-filled rubbers was more sticky and could easily attach to the granite ball, while the wear debris of the silica-reinforced samples was more "dusty-like." Scanning electron microscopic pictures of the debris are shown in Fig. 11 where the carbon black-reinforced debris has the tendency to attach together and form a smear film, while the silica-filled debris stays apart from each other.

It was observed that when the experiment runs for a long period of time, rubber wear particles stick to the granite surface and the tribosystem under study changes. The

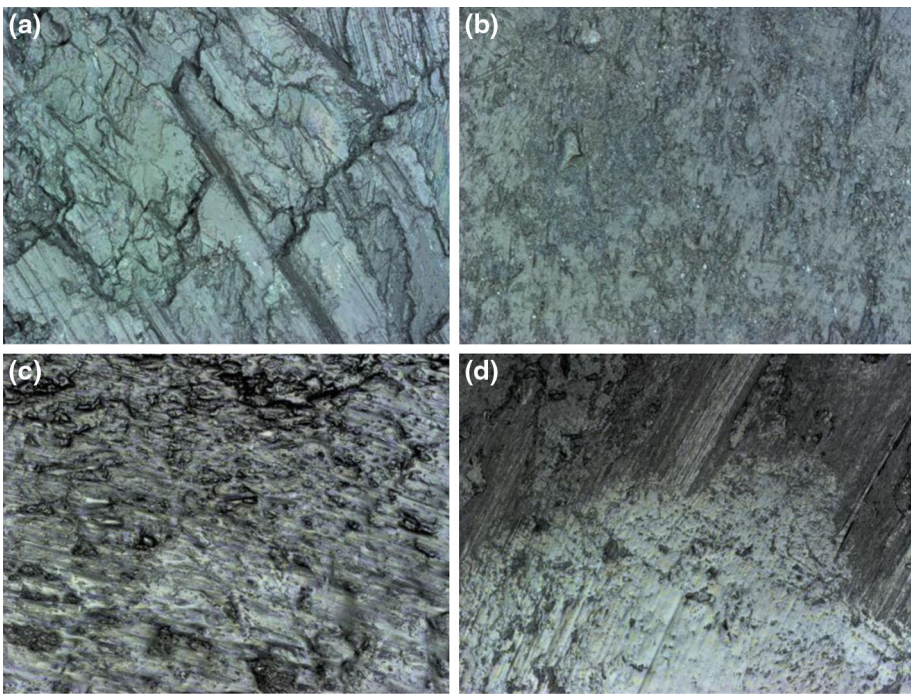

Fig. 13 Confocal microscopic pictures of cleaned rough (**a**), smooth (**b**) and debris attached to the rough (**c**) and smooth (**d**) granite spheres in contact with MC

Fig. 14 Confocal microscopic picture of a polluted rough granite sphere in contact with MS

stabilized measured coefficient of friction when the spheres are contaminated with debris is shown in Fig. 12.

Fresh smooth and rough spheres cleaned by isopropanol as well as wear debris attached spheres (wear debris resulting from the contact of MC sample and spheres) are shown in Fig. 13. The images are made by the laser scanning microscope VK 9700 Keyence on an area of 200 × 286 μm. The debris attached to the rough sphere of MS is shown in Fig. 14. The difference between Figs. 13c and 14 can be explained by Fig. 11. As discussed before, the silica-filled compound's debris shows a tendency to leave the contact area, while carbon black-filled compound's debris mainly sticks to the sphere.

It can be illustrated from Fig. 13 that the wear debris fills the valleys of the sphere, so the contact is between a combination of rubber–rubber as well as rubber–granite at the asperities (depending on the initial roughness and the compound used, the contact is divided in different ratios of rubber–rubber to rubber–granite contact).

A simple comparison between Figs. 7 and 12 shows an increase in the coefficient of friction when the contact region is partially influenced (by the attached wear debris) in all studied tribosystems. The increment in the friction coefficient is dependent on the filler content and filler itself; therefore, the increase in friction for high filler contents is more recognized than for low filled samples. The highest increase in friction level is seen for the HC sample. This is because the carbon black-reinforced rubber debris has a greater tendency to stick to the granite and changes the tribosystem than the silica-filled rubbers. Similar observations have been made in [24, 34, 35]. This situation also occurs in the contact between tire and road. The increase in the friction coefficient can be explained by the modified roughness of the contact as well as modified shearing layers where shearing occurs between a combination of rubber–rubber and rubber–granite in comparison with shear between rubber and granite. In all contacts, the roughness of the granite sphere becomes less because wear debris fills the valleys between the asperities, thus the real area of contact increases; this is seen in Fig. 12. This is more proof of the importance of the real area of contact.

6 Conclusion

A theoretical–experimental approach is used to study the effect of carbon black and silica as reinforcement fillers on friction. DMA measurements showed that carbon black-filled samples have a higher Young's modulus than the silica-filled compounds, and the filler content and the modulus of elasticity are related. Silica-filled rubbers have a higher tan (δ) at lower temperatures and a lower loss tangent at higher temperatures than carbon black-filled compounds, which is a rough indication of higher wet grip and lower rolling resistance for the tire–road contact, respectively.

A ball-on-disk setup was used to conduct friction measurements of six different rubber samples in contact with smooth and rough granite spheres. It was shown theoretically and experimentally that hysteresis has a negligible effect on the coefficient of friction for the smooth counter surface and does play a minor role in the rough surface for the systems studied.

The real area of contact decreases with an increase in elastic modulus as a result of an increase in filler content. On the other hand, the hysteresis increases just slightly with an increase in filler content. Therefore, the real area of contact plays a major role on friction of the studied systems as well as on the interfacial surface layer. In conclusion, because the real area of contact is higher when a smooth sphere is in contact with rubber, and based on the fact that the real area of contact plays the major role in the total friction of granite spheres and rubbers, the coefficient of friction is higher when a smooth sphere is in contact with the rubber samples compared to a rough ball.

Silica-filled samples generally show a higher coefficient of friction than carbon black-filled ones. The coefficient of friction increases with increased filler content for silica-filled rubbers.

The role of wear debris on friction was studied experimentally. It was shown that wear debris attached to the spheres in contact with the rubber samples shows higher friction coefficients. This difference is because of the modified roughness of the balls, as shown in Figs. 13 and 14, and shear stress when rubber is rubbed against rubber or when rubber is rubbed against granite. This research shows the necessity of studying in more detail the nature of shearing a thin surface layer (with modified properties) as the main contributor to the total friction.

Acknowledgments This project is carried out in the framework of the innovation program "GO Gebundelde Innovatiekracht," and funded by the "European Regional Development Fund," "Regio Twente" and "Provincie Overijssel." The project partners Apollo Tyres Global R&D B.V., University of Twente (Tire–Road Consortium), Reef Infra, Stemmer Imaging B.V. and the Provincie Gelderland are gratefully acknowledged.

References

1. Le Gal, A., Yang, X., Klüppel, M.: Evaluation of sliding friction and contact mechanics of elastomers based on dynamic-mechanical analysis. J. Chem. Phys. **123**(1), 014704 (2005)
2. Claeys, X., Jingang, Y., Alvarez, L., Horowitz, R., Canudas de Wit, C., Richard, L.: Tire friction modeling under wet road conditions. In: American Control Conference, vol. 1793, pp. 1794–1799 (2001)
3. Lorenz, B., Persson, B.N.J., Fortunato, G., Giustiniano, M., Baldoni, F.: Rubber friction for tire tread compound on road surfaces. J. Phys. Condens. Matter **25**(9), 095007 (2013)
4. O'Boy, D.J., Dowling, A.P.: Tyre/road interaction noise-numerical noise prediction of a patterned tyre on a rough road surface. J. Sound Vib. **323**(1–2), 270–291 (2009)
5. Brancati, R., Strano, S., Timpone, F.: An analytical model of dissipated viscous and hysteretic energy due to interaction forces in a pneumatic tire: theory and experiments. Mech. Syst. Signal Process. **25**(7), 2785–2795 (2011)
6. Rustighi, E., Elliott, S.J., Finnveden, S., Gulyás, K., Mócsai, T., Danti, M.: Linear stochastic evaluation of tyre vibration due to tyre/road excitation. J. Sound Vib. **310**(4–5), 1112–1127 (2008)
7. Susumu, A., Yukio, T., Toshio, M., Akira, A., Kohki, T., Toshio, K., Mamoru, M., Toshiro, Y.: Investigation of environmental problems caused by studded tires of automobiles using PIXE. Nucl. Inst. Methods Phys. Res. B **3**(1–3), 516–521 (1984)
8. Bond, R., Morton, G.F., Krol, L.H.: A tailor-made polymer for tyre applications. Polymer **25**(1), 132–140 (1984)
9. Grosch, K.A.: The rolling resistance, wear and traction properties of tread compounds. Rubber Chem. Technol. **69**(3), 495–568 (1996)
10. Williams, A.R.: Tyre to road interaction: a case for application of research. Tribol. Int. **17**(5), 235–241 (1984)
11. Golden, J.M.: A molecular theory of adhesive rubber friction. J. Phys. A Math. Gen. **8**(6), 966–979 (1975)
12. Rand, C.J., Crosby, A.J.: Insight into the periodicity of Schallamach waves in soft material friction. Appl. Phys. Lett. **89**(26), 261907 (2006)
13. Tabor, D.: The mechanism of rolling friction. II. The elastic range. Proc. R. Soc. Sci. Lond. Ser. A Math. Phys. Sci. **229**(1), 198–220 (1955). doi:10.2307/99713
14. Moore, D.F.: The Friction and Lubrication of Elastomers. Pergamon Press Oxford, New York (1972)
15. Wriggers, P., Reinelt, J.: Multi-scale approach for frictional contact of elastomers on rough rigid surfaces. Comput. Methods Appl. Mech. Eng. **198**(21–26), 1996–2008 (2009)
16. Persson, B.N.J.: Theory of rubber friction and contact mechanics. J. Chem. Phys. **115**(8), 3840–3861 (2001)
17. Persson, B.N.J.: On the theory of rubber friction. Surf. Sci. **401**(3), 445–454 (1998)
18. Lorenz, B., Persson, B.N.J., Dieluweit, S., Tada, T.: Rubber friction: comparison of theory with experiment. Eur. Phys. J. E **34**(12), 1–11 (2011)
19. Pan, X.D.: Wet sliding friction of elastomer compounds on a rough surface under varied lubrication conditions. Wear **262**(5–6), 707–717 (2007)
20. Patent Application (Michelin). US patent 5,227,425
21. Persson, B.N.J., Albohr, O., Tartaglino, U., Volokitin, A.I., Tosatti, E.: On the nature of surface roughness with application to contact mechanics, sealing, rubber friction and adhesion. J. Phys. Condens. Matter **17**(1), R1–R62 (2005)
22. Persson, B.N.J., Albohr, O., Heinrich, G., Ueba, H.: Crack propagation in rubber-like materials. J. Phys. Condens. Matter **17**(44), R1071–R1142 (2005)
23. Blau, P.J.: Embedding wear models into friction models. Tribol. Lett. **34**(1 SPEC. ISS.), 75–79 (2009)
24. Boissonnet, L., Duffau, B., Montmitonnet, P.: A wear particle-based model of friction in a polymer-metal high pressure contact. Wear **286–287**, 55–65 (2012)
25. Williams, M.L., Landel, R.F., Ferry, J.D.: The temperature dependence of relaxation mechanisms in amorphous polymers and other glass-forming liquids. J. Am. Chem. Soc. **77**(14), 3701–3707 (1955)
26. Ferry, J.D.: Viscoelastic Properties of Polymers. Wiley, New York (1980)
27. Fritzsche, J., Klüppel, M.: Structural dynamics and interfacial properties of filler-reinforced elastomers. J. Phys. Conden. Matter **23**(3), 035104 (2011)
28. Klüppel, M.: Evaluation of viscoelastic master curves of filled elastomers and applications to fracture mechanics. J. Phys. Conden. Matter **21**(3), 035104 (2009)
29. Lorenz, B., Pyckhout-Hintzen, W., Persson, B.N.J.: Master curve of viscoelastic solid: using causality to determine the optimal shifting procedure, and to test the accuracy of measured data. Polymer **55**(2), 565–571 (2014). doi:10.1016/j.polymer.2013.12.033
30. Cochet, P., Barriquand, L., Bomal, Y., Touzet, S.: Precipitated Silica in Tire Tread. Paper presented at the ACS, Rubber Division, Cleveland, OH, Oct. 17–20 (1995)
31. Persson, B.N.J.: Rubber friction: role of the flash temperature. J. Phys. Condens. Matter **18**(32), 7789–7823 (2006)
32. Rodriguez, N.V., Masen, M.A., Schipper, D.J.: Tribologically modified surfaces on elastomeric materials. Proc. Inst. Mech. Eng. Part J J. Eng. Tribol. **227**(5), 398–405 (2013)
33. Momozono, S., Nakamura, K., Kyogoku, K.: Theoretical model for adhesive friction between elastomers and rough solid surfaces. J. Chem. Phys. **132**(11), 114105 (2010)
34. Bahadur, S.: The development of transfer layers and their role in polymer tribology. Wear **245**(1–2), 92–99 (2000)
35. Mergler, Y.J., Schaake, R.P., Huis in't Veld, A.J.: Material transfer of POM in sliding contact. Wear **256**(3–4), 294–301 (2004)